

On the numerical simulation of wellbore pressure in gas reservoirs incorporating the phenomena of slippage, formation damage and wellbore storage

Ricardo Zagos Hermida Garcia de Queiroz¹, Rebeca Costa Dias do Rosário¹, Grazione de Souza¹ and Helio Pedro Amaral Souto¹

¹Departamento de Modelagem Computacional, Universidade do Estado do Rio de Janeiro, Rua Bonfim, 25, Vila Amélia, 28625-570 - Nova Friburgo, RJ, Brazil

Emails: rzagos01@gmail.com, rebecacostadias@gmail.com, gsouza@iprj.uerj.br, helio@iprj.uerj.br

Abstract — In this work, we consider the effects of gas slippage and wellbore storage in shale gas reservoirs. We use the Finite Difference Method for the discretization of the nonlinear governing equation, and the iterative Gauss-Seidel method is applied to obtain the solution of the algebraic system. We also perform pressure tests in the producing well through the use of numerical simulation using cylindrical coordinates. The results, obtained in the well testing analysis context, show the relevance of the introduction of the slip, formation damage and wellbore storage on the flow simulation in shale gas reservoirs.

Keywords — Natural gas, Numerical reservoir simulation, Numerical well testing, Shale gas, Slip flow.

I. INTRODUCTION

Archaeological records show that ancient civilizations in different parts of the world used oil. Incas and Babylonians used the oil to lay bricks, to pave roads, and to waterproof ceramic artifacts [6, 34]. However, it was only in the 20th century that oil began to stand out as economic activity on the world stage, with the emergence of the large automotive industries and oil companies, with the latter beginning the search for more oil reserves. On the other hand, natural gas has been in the background for a long time, mainly due to its specificities concerning transport and storage. However, this situation has changed, mostly in the transition between the 20th and 21st centuries.

The market for natural gas of fossil origin has grown worldwide for several reasons, such as the discovery of new deposits, the lower degree of pollution that its burning causes, when compared to oil, and its diversity of applications. The economic relevance of natural gas was evident in the years 1973 and 1979 when the Organization of Petroleum Exporting Countries (OPEC) raised oil prices to a level that led to changes in hydrocarbon exploration and production and the general dynamics of generation and con-

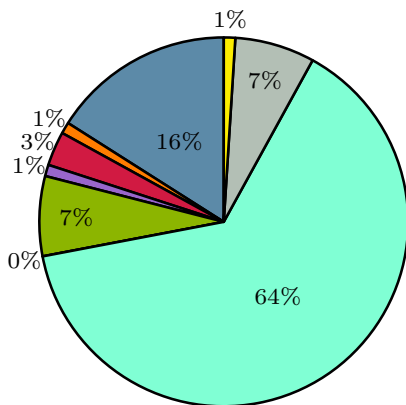
sumption of energy in the world. As a consequence, activities associated with natural gas increased [4]. In this context, Fig. 1 presents the Brazilian energy matrix in the 1970s and 2010. In this figure, we can see that the consumption of natural gas increases from 3 to 9%.

In Brazil, in 1941, natural gas began to appear in the economic scenario due to the discovery of the first commercial oil field in Candeias, Bahia, the industrial sector being its first destination. Due to the adverse effects of the two oil shocks, there was an increase in the production of natural gas due to the exploration and development of the Campos Basin in Rio de Janeiro [9]. At the end of the 1990s, with the completion of the construction of the Bolivia-Brazil gas pipeline (GASBOL) [7], the import of natural gas from Bolivia began, and it consolidated itself as a representative energy source in the Brazilian energy matrix, leaving aside the oil by-product label.

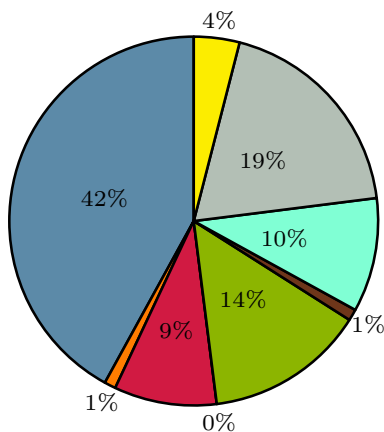
Currently, with the discoveries of pre-salt reserves in the Santos Basin [32], interest in natural gas reserves in Brazil has been growing even more rapidly in recent years. Figure 2 shows the growth of gas production over the years and the dependence on Bo-

livan gas imports, which is necessary to supply national consumption. However, the Energy Research Company (EPE) disclosed, through its National Energy Plan [14], that the national natural gas supply will be adequate to meet the demand of all the commitments assumed until 2030, thus making self-sufficient Brazil in the sector.

Energy Matrix 1970



Energy Matrix 2010



- Petroleum
- Steam coal
- Natural gas
- Metallurgical coal
- Uranium U308
- Firewood
- Hydraulic energy
- Sugarcane products
- Other primary energy

Fig. 1: Brazilian energy matrix in the 1970s and 2010 [15].

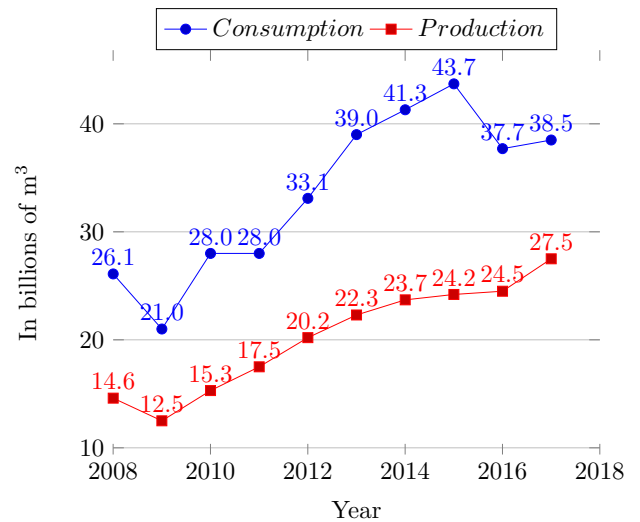


Fig. 2: Gas production and consumption in Brazil between 2008 and 2017 based on the National Energy Balance [19].

1.1. Obtaining natural gas

We define a reservoir of natural gas as a deposit that presents a mixture of hydrocarbons in the gaseous state [17]. As stated by Ezekwe [17], we can classify gas reservoirs as a reservoir of dry gas, wet gas, or retrograde condensation gas, according to the type and behavior of the fluid. When there are no molecules heavy enough to form liquid hydrocarbons after surface separation processes, we say that the reservoir is to be dry gas. We call the deposit a wet gas reservoir when it produces a certain amount of liquid in the well and/or in the surface facilities. In turn, as we produce gas from a retrograde condensation gas reservoir, the pressure decreases, and the temperature remains approximately constant. Thus, there is a liquid phase formation in the reservoir through the condensation of the gas.

Another classification that can be applied is that of conventional and unconventional reservoirs. In conventional gas reservoirs, it is possible to produce from vertical wells while it is required specific production techniques for unconventional reservoirs. For example, we can cite the horizontal wells and hydraulic fracturing since there is higher resistance to the gas flow due to the lower absolute permeability of the reservoir. However, with the advancement of technological development, the gas of unconventional origin began to gain prominence in the world economic scenario. India [21], Brazil [27], and USA [40] are among the ten

nations with the largest reservoirs of shale gas in the world, a type of unconventional reservoir. The trend is that gas of unconventional origin will be essential in the world economy in the coming decades.

Unconventional gas reservoirs can be of different types: deep gas reservoirs (located beyond 4,500 meters in depth); low permeability (tight gas); shale gas; gas adhered to coal veins (coalbed methane); gas from pressurized zones (at very high pressure when compared to other reservoirs with the same depth); and underwater and Arctic hydrates (methane hydrates) [2]. The focus of this work, however, is the shale gas reservoirs.

1.2. Shale gas reservoirs

The shale gas reservoir sedimentary rock has a fine granulometry and very low permeability [22]. Also, the shales have quite variable mineralogical formation, with a predominance of brittle minerals such as quartz, carbonates, and feldspars [20]. Although it has characteristics of unconventional reservoirs, its exploitation has increased over the years.

Hasan et al. [21] has shown that two-thirds of the world's hydrocarbon reserves are unconventional and that this fact is directly related to the growing importance of shale gas in the world energy matrix. On the other hand, Gomes [19] claims that technological advances in the sector are allowing its production to become attractively economical. It has been drilled more than 50,000 wells over two years in gas reservoirs in the United States [28], making the country's hydrocarbon production almost double.

Countries such as the USA and Brazil have a large number of gas reservoirs, which is very important in economic terms and of influence in the international socio-political framework. As a result of the growth in non-conventional gas exploration, these countries' dependence on the world's largest oil and gas producers, such as Venezuela and Russia, can end.

Despite the environmental concern with fossil fuels and the rapid growth in the use of fuels from renewable sources, Jia et al. [22] believe that fossil energy should still account for 78% of global energy consumption in the year 2040. Even though natural gas of fossil origin is not renewable, technological advances in the area and the growth of discoveries of shale gas reservoirs guarantee its use for still many years. Knudsen et al. [24] show that in recent years

the United States has been reducing the use of coal-fired power plants and replacing them with natural gas in the generation of electricity. In part, we can explain this by the desire to reduce emissions of polluting carbon dioxide, which harms the environment so much.

Wellbore Testing Analysis studies the pressure and flow changes as a function of production time, through measurements at the bottom of the well and the flow at the surface. From the measured pressure response, it is possible to determine the reservoir properties useful for production planning [41]. In a well test, a transient pressure response occurs due to a production/injection flow. Depending on the objectives of the test, we record the response of the well over a relatively short period when compared to the productive life of the reservoir. In this work, in addition to a sensitivity analysis, well pressure tests using numerical simulation is also done.

II. POROUS MEDIA GAS FLOW

Petroleum is a mixture of hydrocarbons, which has its physical state-properties determined, in general, by its composition, temperature (T), and pressure (p). According to Ezekwe [17], oil is the part that remains in the liquid state when a mixture of hydrocarbons is brought from the reservoir conditions to the surface conditions, while the natural gas presents the gaseous state in the surface conditions. Under reservoir conditions, natural gas can be present in gaseous form or dissolved in oil.

Regarding the composition of natural gas, the amount of each component can vary depending on the type of reservoir and its characteristics, for example, the location (land or sea), the type of soil, and the geological formation process of the basin, among other factors [30]. However, as can be seen in Table 1 which presents the typical composition of a natural gas reservoir, it is evident that the primary component is methane, which may represent an amount of 70 to 98% of the total natural gas, and in smaller quantities, considered as impurities, carbon dioxide, hydrogen sulfide, and nitrogen. Besides temperature and pressure conditions, another fundamental parameter for calculating the properties of the gas is its relative density (or specific gravity), γ , which is the ratio between the molecular mass of the gas, M , and the molecular mass of air, M_{air} . In this work, it is considered a reservoir of dry gas, produced without the

appearance of liquid at any time of production.

Table 1: Typical chemical composition of natural gas

| Component | Composition |
|--------------------------------|-------------|
| N ₂ | up to 15% |
| CO ₂ | up to 5% |
| H ₂ S | up to 3% |
| He | up to 5% |
| CH ₄ | 70-80% |
| C ₂ H ₆ | 1-10% |
| C ₃ H ₈ | up to 5% |
| C ₄ H ₁₀ | up to 2% |
| C ₅ H ₁₂ | up to 1% |
| C ₆ H ₁₄ | up to 0.5% |
| C ₇₊ | up to 0.5% |

For gas mixtures of hydrocarbons, we use the pseudo-critical pressure and temperature coordinates, p_{pc} and T_{pc} , respectively, to determine the so-called pseudo-reduced coordinates [26], and we use them to calculate the physical properties of natural gas.

Sutton [38] presents, depending on the gas density, the correlations that we apply here to obtain the pseudo-critical pressure and temperature, which are fundamental for the reservoir simulations [16]. We use them in determining, for example, the compressibility factor (Z), volume formation factor (B) and viscosity (μ) [37]. From Z and the universal gas constant, R , it is possible to determine the density, ρ , from the equation of state for a real gas, $\rho = pM/ZRT$.

The gas volume formation factor is the relationship between the volumes it occupies under reservoir conditions (V) and standard conditions (V_{sc}) (pressure, p_{sc} , and temperature, T_{sc} , in standard conditions) [16]. Thus, $B = p_{sc}ZT/pT_{sc}$ whereas $Z_{sc} \approx 1$.

On the other hand, we calculate the viscosity of natural gas using the correlation suggested by Lee et al. [25], widely used in reservoir simulation.

Here, the effective porosity (ϕ) varies depending on the pressure [16]:

$$\phi = \phi^0 [1 + c_\phi (p - p^0)] \quad (1)$$

where ϕ^0 and p^0 are, respectively, the porosity and pressure in the reference conditions. c_ϕ is the coefficient of compressibility of the rock, and we assume

that the compressibility of the rock is small and constant.

In addition to porosity, the economic viability of a reservoir also depends on the permeability of the rock. This property is a measure of a porous material's ability to allow fluids to pass through its pores. We usually represent the absolute permeability by the tensor k .

2.1. Slip in gas flow

Studies and predictions about the flow of gas in porous media are more difficult to carry out than those of liquid because the gas properties generally depend more strongly on pressure and also due to the different mass transport mechanisms that can be present [28, 31]. Therefore, in some cases, the classic Darcy's law does not adequately describe the flow physics, and experimental data suggest corrections for the calculation of permeability and, thus, we introduce a modified Darcy's law [28]

$$\mathbf{v} = -\frac{\mathbf{k}_a}{\mu} (\nabla p - \rho g \nabla D), \quad (2)$$

where \mathbf{k}_a is the apparent permeability tensor, \mathbf{v} is the surface velocity of the fluid, g is the acceleration of gravity and D is the depth.

Specifically for gases, the slip flow regime occurs when the average free path of the gas molecules has a scale comparable to the pore size [18]. So, both the reservoir and fluid properties influence the determination of apparent permeability. We can mention, among the non-Darcy effects, that we can incorporate in the apparent permeability, high flow rates (inertial and turbulent effects), non-Newtonian fluid flow (for liquids), and slip flow, which occurs only for gas under certain reservoir conditions [5].

When the fluid is a gas, the Klinkenberg effect shows that the permeability measurements made in the laboratory result in values higher than the absolute values, due to the slipping of the gas on the walls of the porous medium. This slip results in a higher flow and leads to a correction of the apparent permeability [23],

$$\mathbf{k}_a = \left(1 + \frac{b}{p}\right) \mathbf{k} \quad (3)$$

where b is the Klinkenberg parameter and \mathbf{k} the absolute permeability tensor.

In reality, the mass is transported in the porous medium by a variety of mechanisms, one of which is the so-called Knudsen diffusion. The Knudsen number measures the relationship between the mean free path of the molecules, λ , and the characteristic pore length, R_h , so that $Kn = \lambda/R_h$, where $\lambda = (\mu/p)\sqrt{\pi ZRT/(2M)}$, $R_h = 2\sqrt{2}\tau\sqrt{k/\phi}$, and τ is the tortuosity of the porous medium.

The slip flow regime occurs for $10^{-3} < Kn < 0.1$ and we can also introduce a different model for determining apparent permeability [28]

$$k_a = \left(1 + \frac{4Kn}{1 + Kn}\right) k = f(Kn)k. \quad (4)$$

2.2. Governing equation

In obtaining the partial differential equation (PDE) that governs the isothermal flow of a gas in a porous medium, we employ the mass conservation equation and the modified Darcy's law. We also take into account the effects of slippage, wellbore storage and formation damage, disregarding the phenomenon of gas adsorption, the gravitational force and non-Darcy behaviors related to inertial effects.

As it takes time to the hydrocarbons in the reservoir to reach the surface, in the first moments, we produce the fluid initially stored in the well. This effect is called wellbore storage. The formation damage concerns the reduction of permeability in the region close to the well, caused by wellbore fluids used during drilling and completion.

According to Li et al. [29], mass conservation for the flow of gas in porous media can be described, excluding the adsorption effects and source terms [3], by

$$\frac{\partial}{\partial t} \left(\frac{\rho_{sc}\phi}{B} \right) + \nabla \cdot \left(\frac{\rho_{sc}\mathbf{v}}{B} \right) = 0. \quad (5)$$

Then, replacing Eq. (2) in Eq. (5) and ignoring the effects of gravity due to the low specific gravity of the gas and the thickness of the reservoir,

$$\nabla \cdot \left(\frac{\mathbf{k}_a}{\mu B} \nabla p \right) = \frac{\partial}{\partial t} \left(\frac{\phi}{B} \right). \quad (6)$$

We can rewrite the term $\partial(\phi/B)/\partial t$ if we take into

account the fluid and rock properties [13]

$$\begin{aligned} \frac{\partial}{\partial t} \left(\frac{\phi}{B} \right) &= \frac{1}{B} \frac{d\phi}{dp} \frac{\partial p}{\partial t} + \phi \frac{d}{dp} \left(\frac{1}{B} \right) \frac{\partial p}{\partial t} \\ &= \left[\frac{c_\phi \phi^0}{B} + \phi \frac{d}{dp} \left(\frac{1}{B} \right) \right] \frac{\partial p}{\partial t} \\ &= \Gamma_p \frac{\partial p}{\partial t}, \end{aligned} \quad (7)$$

where we also employed Eq. (1).

To study the flow dynamics in the region close to the producing well, we assume a two-dimensional flow in cylindrical geometry in the rz -plan and a diagonal permeability tensor, so that:

$$\frac{1}{r} \frac{\partial}{\partial r} \left(\frac{k_{ar}}{\mu B} \frac{\partial p}{\partial r} \right) + \frac{\partial}{\partial z} \left(\frac{k_{az}}{\mu B} \frac{\partial p}{\partial z} \right) = \Gamma_p \frac{\partial p}{\partial t}. \quad (8)$$

where k_{ar} and k_{az} are the apparent permeabilities in the r - and z - directions, respectively.

As we are considering the effects of storage in the well, the production flow in it is given by [29]

$$Q_{sc} = q_{sc} + C_{sc} \frac{dp_{wf}}{dt}, \quad (9)$$

where q_{sc} is the flow from the porous medium, C_{sc} is the storage coefficient (that already incorporates B) and p_{wf} the pressure in the well. The flow rate q_{sc} is calculated by [35]

$$q_{sc} = -J_w (p - p_{wf}), \quad (10)$$

where J_w is the productivity index.

Finally, as an initial condition we impose

$$p(r, z, t = 0) = p_{ini}(r, z) = p_{ini}, \quad (11)$$

where p_{ini} represents the initial pressure before the reservoir undergoes any changes due to fluid production/injection.

On the other hand, the external boundary conditions are of null flow at the external borders,

$$\left(\frac{\partial p}{\partial z} \right)_{z=0, L_z} = \left(\frac{\partial p}{\partial r} \right)_{r=r_e} = 0, \quad (12)$$

where L_z is the thickness of the reservoir and r_e is the outer radius of the reservoir. In turn, for the internal boundary condition,

$$\left(\frac{\partial p}{\partial r} \right)_{r=r_w} = -\frac{q_{sc} B \mu}{2\pi k_{ar} h r_w} \quad (13)$$

where h is the thickness of the production region considered and r_w is the radius of the well.

III. NUMERICAL RESOLUTION METHODOLOGY

We employ a computational mesh of centered blocks [1, 5, 10, 16] and the cylindrical coordinate system (r and z), Fig. 3, and we also assume the angular symmetry of the flow. We obtain the numerical solution in the nodes of the computational mesh, located in the centers of the cells, with n_r and n_z being the numbers of cells in the r - and z - directions, respectively. We also use fractional indexes $i \pm 1/2$ and $k \pm 1/2$ to indicate cell interfaces of the computational mesh.

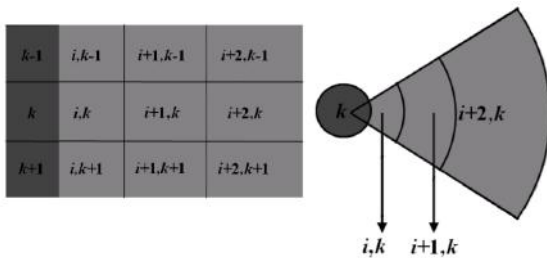


Fig. 3: Two-dimensional cylindrical domain discretized.

So, for the cell i, k and the time $n + 1$ we can write that

$$V_{i,k} \left(\Gamma_p \frac{\partial p}{\partial t} \right)_{i,k}^{n+1} = V_{i,k} \left[\frac{1}{r} \frac{\partial}{\partial r} \left(\mathbb{T}_r \frac{\partial p}{\partial r} \right) \Delta r + \frac{\partial}{\partial z} \left(\mathbb{T}_z \frac{\partial p}{\partial z} \right) \Delta z \right]_{i,k}^{n+1} \quad (14)$$

where the governing equation was multiplied by the volume of the cell, $V_{i,k}$, and \mathbb{T} stands for the transmissibility.

Following the techniques traditionally applied in reservoir simulation [5, 16] and employing centered differences

$$V_{i,k} \frac{\partial}{\partial r} \left(\mathbb{T}_r \frac{\partial p}{\partial r} \right)_{i,k}^{n+1} \cong \frac{V_{i,k}}{\Delta r_{i,k}} \left[\left(\mathbb{T}_r \frac{\partial p}{\partial r} \right)_{i+\frac{1}{2},k} - \left(\mathbb{T}_r \frac{\partial p}{\partial r} \right)_{i-\frac{1}{2},k} \right]^{n+1} \quad (15)$$

and

$$V_{i,k} \frac{\partial}{\partial z} \left(\mathbb{T}_z \frac{\partial p}{\partial z} \right)_{i,k}^{n+1} \cong \frac{V_{i,k}}{\Delta z_{i,k}} \left[\left(\mathbb{T}_z \frac{\partial p}{\partial z} \right)_{i,k+\frac{1}{2}} - \left(\mathbb{T}_z \frac{\partial p}{\partial z} \right)_{i,k-\frac{1}{2}} \right]^{n+1} \quad (16)$$

Similarly, for the discretization of pressure derivatives in the r -direction,

$$\left(\frac{\partial p}{\partial r} \right)_{i+\frac{1}{2},k}^{n+1} \cong \frac{p_{i+1,k}^{n+1} - p_{i,k}^{n+1}}{\Delta r_{i+\frac{1}{2},k}} \quad (17)$$

and

$$\left(\frac{\partial p}{\partial r} \right)_{i-\frac{1}{2},k}^{n+1} \cong \frac{p_{i,k}^{n+1} - p_{i-1,k}^{n+1}}{\Delta r_{i-\frac{1}{2},k}} \quad (18)$$

where $\Delta r_{i \pm 1/2, k}$ is the distance between nodes of cells i, k and $i \pm 1, k$. We can obtain approximations for the derivatives in the z -direction analogously.

In the case of the accumulation term, we employ a conservative expansion [16]

$$\Gamma_{p,i,k}^{n+1} = V_{i,k} \left[\frac{1}{B^n} \frac{d\phi}{dp} + \phi^{n+1} \frac{d}{dp} \left(\frac{1}{B} \right) \right]_{i,k}, \quad (19)$$

where Δt is the time step.

Next, we obtain a totally implicit formulation for Eq. (14) using a backward Euler approximation,

$$\left(\frac{\partial p}{\partial t} \right)_{i,k}^{n+1} \cong \frac{p_{i,k}^{n+1} - p_{i,k}^n}{\Delta t} \quad (20)$$

3.1. Grid refinement

For an accurate determination of the pressure gradient, we use to construct the non-uniform mesh in the r -direction (where we suppress k for simplicity of notation) [16],

$$\alpha = \left(\frac{r_e}{r_w} \right)^{n_r-1} \quad (21)$$

such as:

1. we space pressure calculation points using

$$r_{i+1} = \alpha_{lg} r_i \quad (22)$$

where $i = 1, 2, \dots, n_r - 1$;

2. we define cell boundaries through

$$r_{i+1/2} = \frac{r_{i+1} - r_i}{\log_e(r_{i+1}/r_i)} \quad (23)$$

where $i = 1, 2, \dots, n_r - 1$; and

3. we calculate cell volumes employing

$$r_{i+1/2}^2 = \frac{r_{i+1}^2 - r_i^2}{\ln(r_{i+1}^2/r_i^2)} \quad (24)$$

In the case of the z -direction, we use $\Delta z = L_z/n_z$.

We now introduce the definitions of transmissibilities:

$$T_{r,i\pm\frac{1}{2},k}^{n+1} = \left(\frac{G_{r,i\pm\frac{1}{2},k}^{n+1}}{\mu B} \right)_{i\pm\frac{1}{2},k}^{n+1}, \quad (25)$$

and

$$T_{z,i,k\pm\frac{1}{2}}^{n+1} = \left(\frac{G_{z,i,k\pm\frac{1}{2}}^{n+1}}{\mu B} \right)_{i,k\pm\frac{1}{2}}^{n+1}, \quad (26)$$

where, considering that the total angle is 2π and the apparent permeabilities [16],

$$G_{r,i\pm\frac{1}{2},k}^{n+1} = \frac{\pi \Delta z_k}{\frac{1}{k_{ar,i,k}} \log_e \left(\frac{r_{i+\frac{1}{2}}}{r_i} \right) + \frac{1}{k_{ar,i+1,k}} \log_e \left(\frac{r_{i+1}}{r_{i+\frac{1}{2}}} \right)} \quad (27)$$

and

$$G_{z,i,k\pm\frac{1}{2}}^{n+1} = \frac{\pi \left(r_{i+\frac{1}{2}}^2 - r_{i-\frac{1}{2}}^2 \right)}{\frac{z_{k+\frac{1}{2}} - z_k}{k_{az,i,k}} + \frac{z_{k+1} - z_{k+\frac{1}{2}}}{k_{az,i,k+1}}}, \quad (28)$$

and we apply arithmetic mean to calculate the fluid properties [16].

3.2. Numerical approximation for storage

When we consider the wellbore storage effect, the total flow rate is determined as proposed by Li et al. [29] and Tavares [39]:

$$Q_{sc} = - \sum_{i=K1}^{i=K2} (q_{sc})_{i,k}^{n+1} + C_{sc}^{n+1} \left(\frac{p_{wf}^{n+1} - p_{wf}^n}{\Delta t} \right) \quad (29)$$

with

$$J_w = \frac{k_{ar} \Delta z T_{sc}}{p_{sc} T \ln \left(\frac{r_o}{r_w} \right)} \quad (30)$$

where

$$r_o = \sqrt{r_{1+\frac{1}{2}} r_w}. \quad (31)$$

3.3. The solution of the system of equations

After the process of discretizing the governing equation, as the resulting algebraic equations are non-linear, we must apply a linearization technique,

and we chose the method of Picard [33]. So this results in

$$\begin{aligned} & T_z \Big|_{i,k-1/2}^{v,n+1} p_{i,k-1}^{v+1,n+1} + T_r \Big|_{i-1/2,k}^{v,n+1} p_{i-1,k}^{v+1,n+1} \\ & + T_r \Big|_{i+1/2,k}^{v,n+1} p_{i+1,k}^{v+1,n+1} + T_z \Big|_{i,k+1/2}^{v,n+1} p_{i,k+1}^{v+1,n+1} \\ & - \left[T_z \Big|_{i,k-1/2}^{v,n+1} + T_r \Big|_{i-1/2,k}^{v,n+1} + \left(\frac{\Gamma_p}{\Delta t} \right)_{i,k}^{v,n+1} \right. \\ & \left. + T_r \Big|_{i+1/2,k}^{v,n+1} + T_z \Big|_{i,k+1/2}^{v,n+1} \right] p_{i,k}^{v+1,n+1} \\ & = - \left(\frac{\Gamma_p}{\Delta t} \right)_{i,k}^{v,n+1} p_{i,k}^n \end{aligned} \quad (32)$$

where the index v refers to the previous iterative level when obtaining the pressure. As we can see, the properties and coefficients of the discretized equation are determined at the iterative level v and used after to calculate the new pressure values at the iterative level $v + 1, n + 1$.

In the case of cells in direct contact with the well, we determine its pressure (p_{wf}) through Eq. (10) for a prescribed flow rate.

In solving the linearized system, to obtain the pressures in the porous medium and the well, it was chosen to use the Gauss-Seidel iterative method [16, 36].

IV. NUMERICAL RESULTS

In all numerical simulations, we adopted an arrangement consisting of a vertical producer well, of length L_{wf} and centered on the $r\theta$ -plane, a maximum production time (t_{max}), and an initial time step (Δt_{ini}). The time step can vary depending on the growth rate ($\delta_{\Delta t}$). This methodology allows a growing time step, and we use it until the final time step (Δt_{max}), pre-established, is reached. It is of general use in reservoir simulation [1, 16]. We aim to enhance the accuracy of the calculated well pressure in the initial moments when the pressure drop is more accentuated.

We obtain the results using a standard set of data, based on the non-Darcy model discussed in Li et al. [29], in which the authors incorporated the slippage effect into the apparent permeability. Table 2 shows the parameters for the standard case, and we choose the physical properties as stated by Li et al. [29] (shale gas), and by de Souza [12], which simulated the flow of natural gas, using cylindrical coordinates, to assess

the pressure of a producer well (vertical). As a simplification, we took C_{sc}^{n+1} as constant and equal to C_{sc} (we intend to modify this in future work).

Table 2: Parameters for the standard case.

| Parameter | Value | Unit |
|---------------------|---------------------|-------------------------------|
| c_ϕ | $1.0 \cdot 10^{-6}$ | psi ⁻¹ |
| C_{sc} | 0.7 | scf/psi |
| k_r and k_z | $4.0 \cdot 10^{-6}$ | Darcy |
| L_r | 1,250 | ft |
| L_z | 40.0 | ft |
| L_{wf} | 40.0 | ft |
| n_r | 40 | — |
| n_z | 3 | — |
| p_{ini} and p^0 | 4,500 | psi |
| p_{sc} | 14.65 | psi |
| Q_{sc} | $-1.0 \cdot 10^4$ | scf/day |
| R | 10.73 | ft ³ psi/R lbm-mol |
| t_{max} | 375 | day |
| tol | $1.0 \cdot 10^{-6}$ | psi |
| T | 609.67 | R |
| T_{sc} | 519.67 | R |
| γ | 0.6 | — |
| $\delta_{\Delta t}$ | 1.1 | — |
| Δt_{ini} | 0.0001 | day |
| Δt_{max} | 10.0 | day |
| τ | 1.41 | — |
| ϕ and ϕ^0 | 0.12 | — |

4.1. Numerical verification

We employed different meshes in the study of numerical convergence: Meshes 1, 2, 3, and 4 with $n_r = 10, 20, 40,$ and 80 cells, respectively. We kept, in all simulations, n_z constant and equal to 3.

Figures 4 and 5 bring the results for the four meshes mentioned in the last paragraph. The results show the pressure in the well as a function of time, obtained considering a production time equal to 375 days. For this purpose, we use specialized and diagnostic graphics, respectively. By the way, in this work, on the diagnostic plots, continuous lines represent pressure drop, and dashed lines represent Bourdet derivative [8].

From the figures, we can see that we achieve numerical convergence as the number of cells n_r increases, with the consequent overlap of pressure curves. Then, as a consequence of the results ob-

tained, the 40 cells mesh was adopted as the standard (lowest computational cost). From the pressure curves in Fig. 4, we realize that we capture two typical regimes: a nearly horizontal line that corresponds to the storage in the well and an inclined straight line related to the transient flow regime. However, the effects of external borders are still absent, reflecting the fact that the pressure at the reservoir frontier ($r = r_e$) remains equal to the pressure p_{ini} . From the Bourdet derivative (Fig. 5), we can more clearly distinguish the two distinct flow regimes. First, we observe the inclined line related to the wellbore storage and after a straight line corresponding to the transient flow regime, without boundary effects.

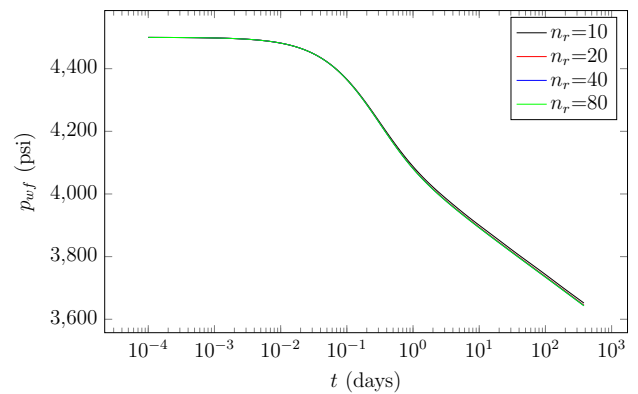


Fig. 4: Numerical convergence under grid refinement, specialized plot.

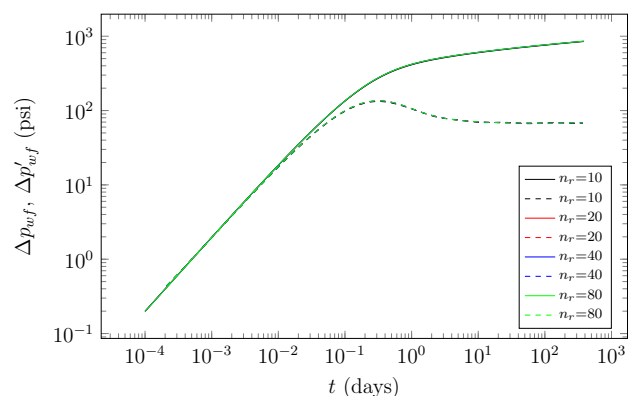


Fig. 5: Numerical convergence under grid refinement, diagnostic plot.

We also carried out tests to observe the behavior of the solution concerning the variation of the time step $\Delta t^{n+1} = \delta_{\Delta t} \Delta t^n$. We consider two situations for prescribed Δt_{ini} and Δt_{max} : numerical simulations

with $\delta_{\Delta t} = 1$, Figs. 6 and 7, and pressure curves calculated with a variable $\delta_{\Delta t}$ ($\delta_{\Delta t} \neq 1$), Figs. 8 and 9, respectively.

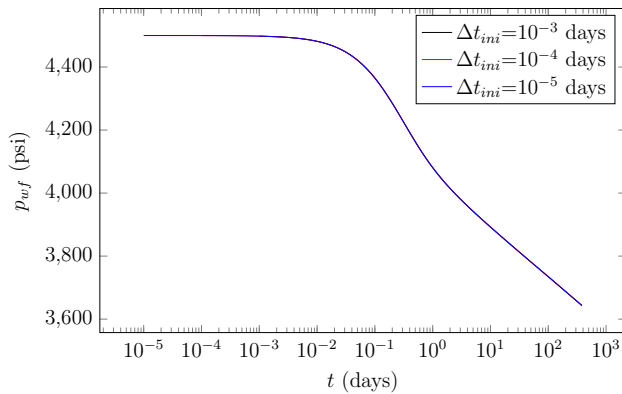


Fig. 6: Wellbore pressure variation as a function of time step, specialized plot.

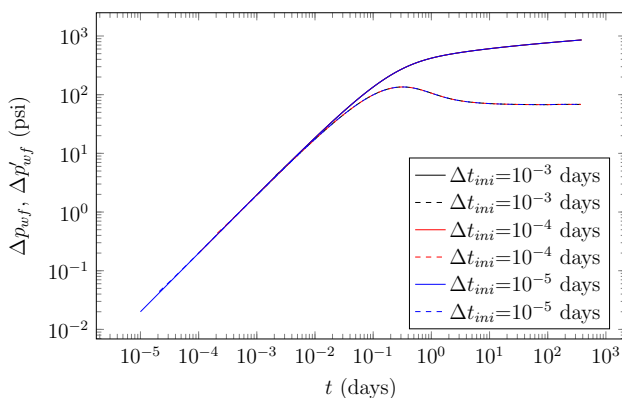


Fig. 7: Wellbore pressure variation as a function of time step, diagnostic plot.

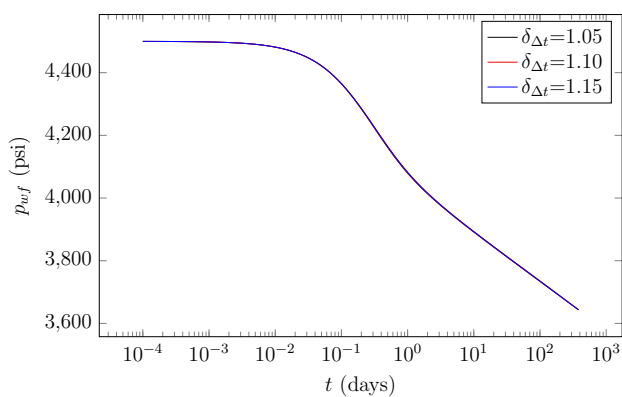


Fig. 8: Wellbore pressure variation due to the growth of Δt , specialized plot.

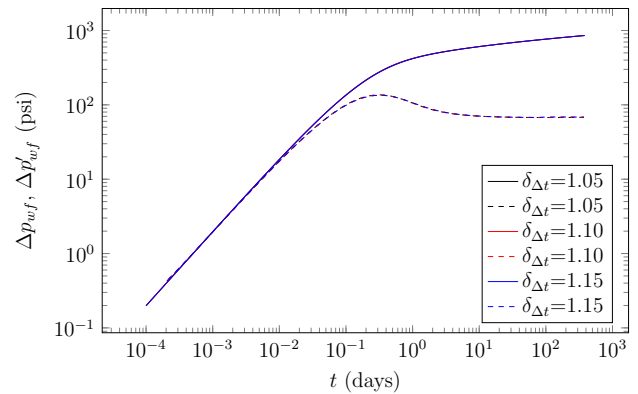


Fig. 9: Well pressure variation due to the growth of Δt , diagnostic plot.

As we can see from these figures, the results did not show significant variations concerning changes in the well pressure and pressure derivative when we employ these Δt_{ini} and δt values. Based on this verification, we established the standard values for the initial time step, the growth rate, and the maximum time step of Table 2. As already mentioned, the use of a small initial time step contributes to enabling the analysis of the pressure variation in the initial moments of production (typical in Well Test Analysis using numerical simulation).

We also studied the effect of the tolerance used to stipulate convergence in the internal (Gauss-Seidel method) and external (Picard method) iterations. Figures 10 and 11 present the results, which corroborate the choice of tolerance for the standard case since we did not detect significant differences in the results.

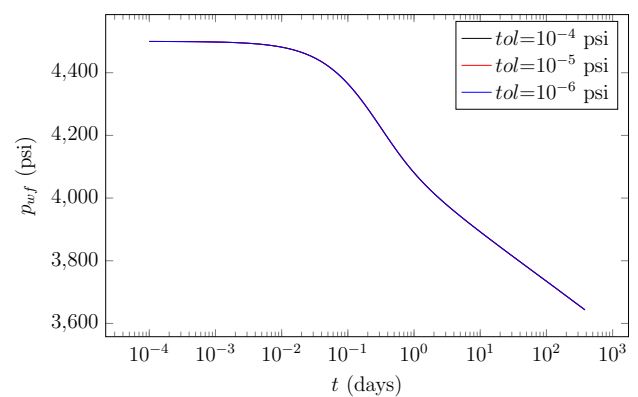


Fig. 10: Wellbore pressure variation as a function of tolerance, specialized plot.

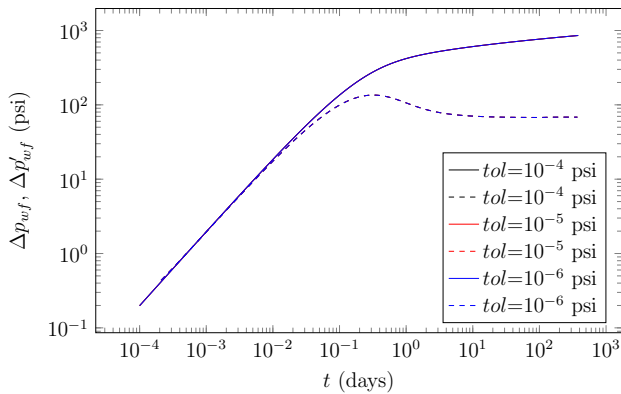


Fig. 11: Wellbore pressure variation as a function of tolerance, diagnostic plot.

As an additional check, Figs. 12 (specialized plot) and 13 (diagnostic plot) show our results obtained with higher values for porosity and permeability, 0.2 and $1.0 \cdot 10^{-3}$ Darcy respectively, and without taking into account the phenomena of slippage, formation damage, and wellbore storage.

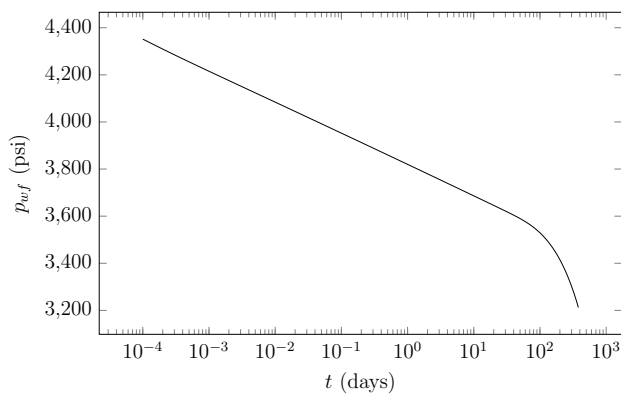


Fig. 12: Well pressure variation for higher permeability and porosity, and Darcy's flow, specialized plot.

This simulation is the same as those performed by de Souza [12] for the flow considering only the classic Darcy law, whose results were verified through a direct confrontation with those obtained with the commercial simulator IMEX/CMG [11]. IMEX is a commercial simulator widely known and used in reservoir simulation.

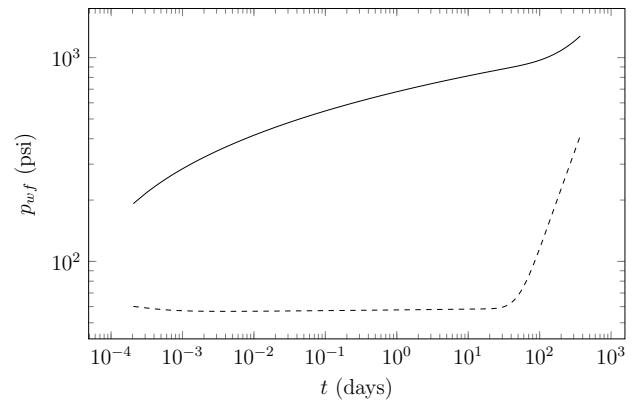


Fig. 13: Wellbore pressure variation for higher permeability and porosity, and Darcy's flow, diagnostic plot.

The values here numerically calculated accurately reproduce those determined by de Souza [12]. Therefore, indirectly, it was possible to validate our simulator in the case of flow governed by the classic Darcy law, without the effects of slippage, formation damage, and wellbore storage.

4.2. Sensitivity analysis

We begin by the sensitivity analysis of the effects on the wellbore pressure when we change the reservoir's permeability. In Figs. 14 and 15, we can observe the specialized and diagnostic plots for wellbore pressure variation.

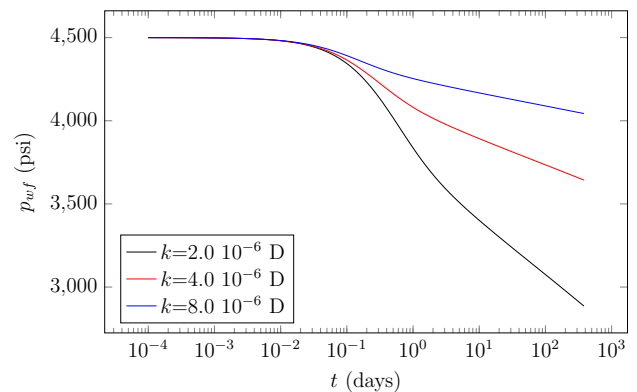


Fig. 14: Wellbore pressure variation as a function of absolute permeability, specialized plot.

The higher the permeability, the lower the pressure drop, following the modified Darcy's law. It is worth mentioning that permeability has a significant impact on flow in porous media, and is often responsible for defining the economic viability of the reser-

voir, including decision making on a hydraulic fracturing operation. In the case of reservoirs, where the slip flow regime occurs, the permeability value also influences Kn, and the Knudsen number increases if we decrease it, with a consequent increase in the apparent permeability value. We also noticed that the higher the permeability, the shorter the duration of the transition for the transient regime.

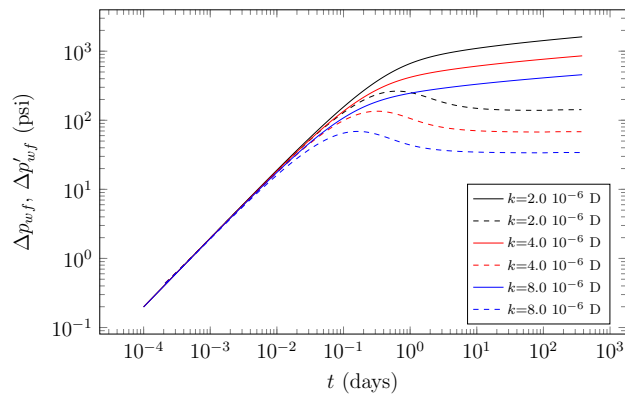


Fig. 15: Wellbore pressure variation as a function of absolute permeability, diagnostic plot.

In this test, and for all curves, we note that boundary effects are absent. We can verify this by inspecting the end of the transient flow regime curve, in the specialized plot, and the curve corresponding to the transient flow regime in the diagnostic plot (Bourdet derivative). Besides that, we can highlight that wellbore storage physically depends on permeability in a way that for lower permeability, wellbore storage effect is more prolonged.

Just as we did with permeability, we used different porosity values to check its influence in the wellbore pressure variation. We show the results in Figs. 16 and 17.

However, for the porosity values that we retained, we only note small variations in the well pressure curves (p_{wf}). From the figures, we observe that higher porosity values lead to lower pressure drop for maximum production time, and this is due to the higher volume of gas that we can produce. Therefore, in this situation, the well pressure drops less for a fixed production flow rate. Porosity also influences the value of the Knudsen number but acting in the opposite direction. Regarding the boundary effects, the smaller the porosity, the shorter the transient flow regime. Moreover, as expected, more significant well-

bore storage effects occur for lower porosity values, although we only capture slight differences for the values used in simulations.

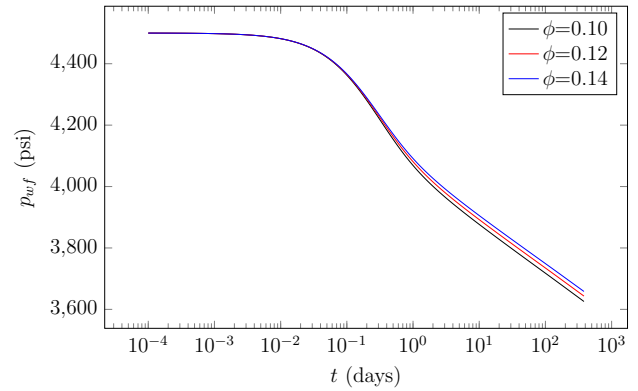


Fig. 16: Wellbore pressure variation as a function of porosity, specialized plot.

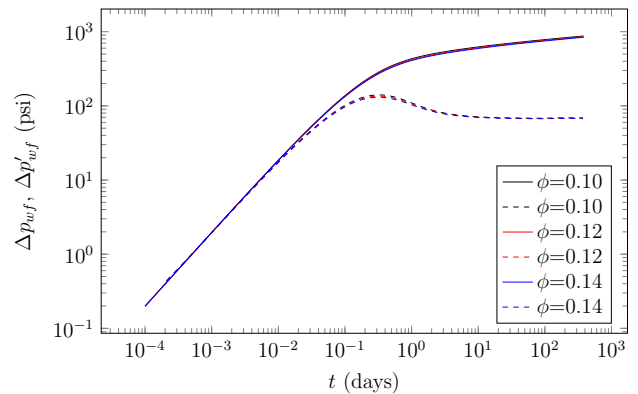


Fig. 17: Wellbore pressure variation as a function of porosity, diagnostic plot.

On the other hand, changing the tortuosity leads only to slight changes in the pressure values for the range that we considered (see Figs. 18 and 19).

We note from the results in Fig. 18 a higher pressure drop as the value of tortuosity increases. This is consistent with the fact that the higher the tortuosity of the medium, the lower the apparent permeability must be and, therefore, the higher the flow resistance.

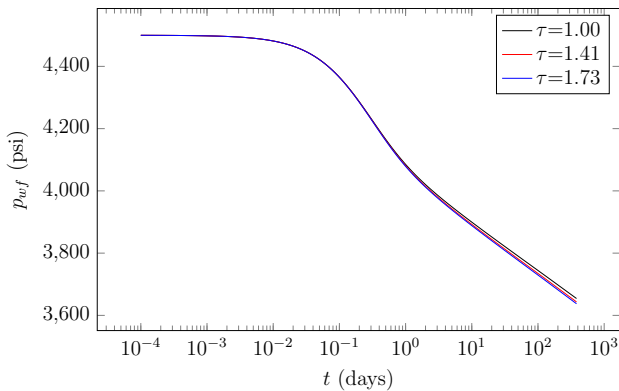


Fig. 18: Wellbore pressure variation as a function of tortuosity, specialized plot.

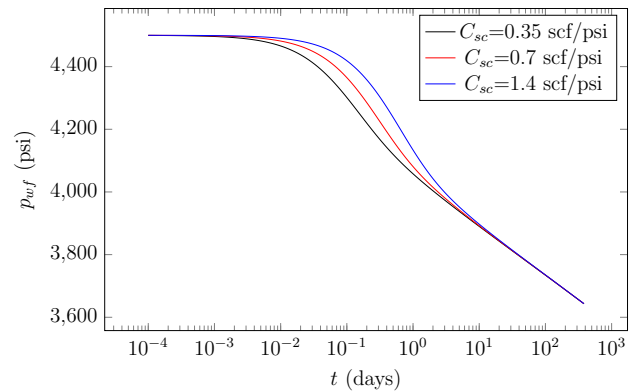


Fig. 20: Wellbore pressure variation as a function of storage, specialized plot.

From the results shown in these figures, we realize that we did not detect significant differences in the Bourdet derivative for this input simulation data.

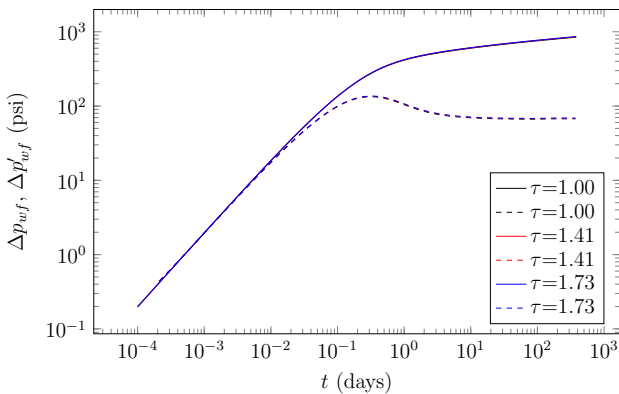


Fig. 19: Wellbore pressure variation as a function of tortuosity, diagnostic plot.

The diagnostic plot (Fig. 21) shows that the wellbore storage strongly influences the results in the initial times, in both the pressure drop and pressure derivative. The higher the wellbore storage, the smaller the pressure drop and the later the transient flow regime will be.

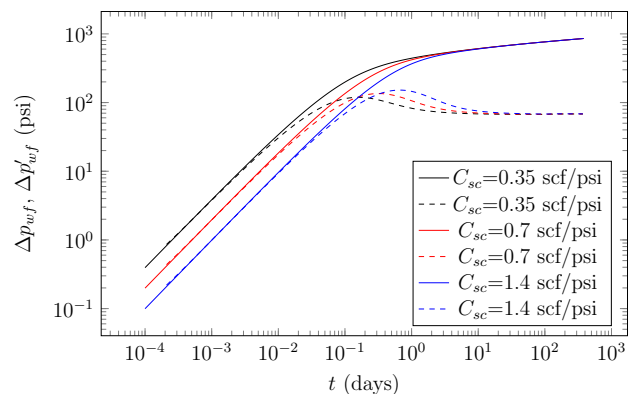


Fig. 21: Wellbore pressure variation as a function of storage, diagnostic plot.

4.3. Well Test Analysis

We now focus on the specific cases of well test analysis. The initial transient response, during a well test, comes from the pressure difference applied to the volume of fluid initially present in the well.

Figure 20 shows the storage effect on pressure behavior in the well. The higher the storage effect, the smaller the representative range of the transient flow regime. This means that a well test must be long enough for the storage effects to disappear so that the flow recorded in the well test identifies the transient regime of reservoir production. In practice, it is from the well test that we obtain the data for the characterization of the well-reservoir system.

We also notice significant results when comparing the pressure variation for the flow without ($k_a = k$) and with the slippage effects ($k_a = f(Kn)k$). The same simulation conditions and parameters were maintained for both models, varying only the property of interest.

Initially, only the responses resulting from the slip flow effect are studied, Fig. 22. Despite presenting a similar initial behavior (storage and transition to the transient regime), the model taking into account the phenomenon of slippage presents a lower pressure drop as production time increases. We can explain

this by the increase in apparent permeability due to the change in the Knudsen number.

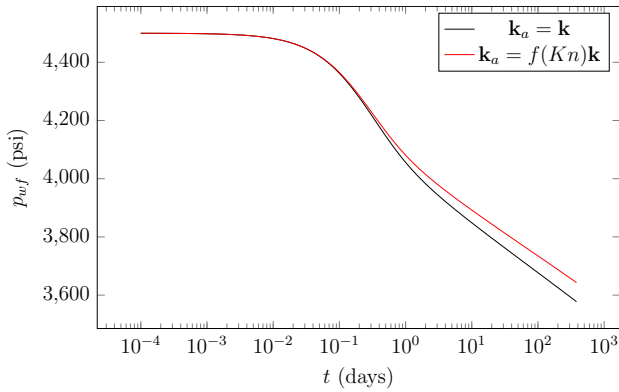


Fig. 22: Well pressure variation depending on gas slippage, specialized plot.

Based on the results in Fig. 23, we note that the use of the classical Darcy’s law (lower apparent permeability) leads to wellbore storage more significant in magnitude and duration.

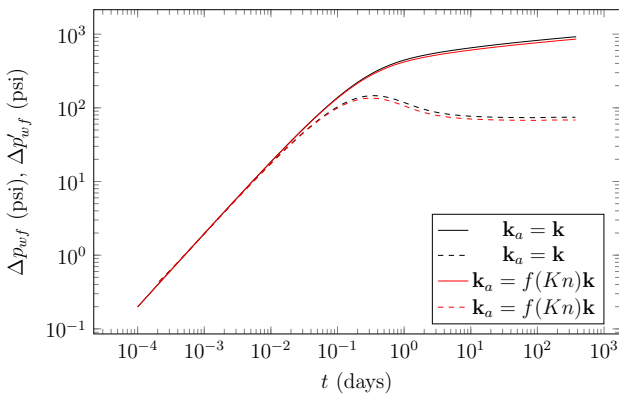


Fig. 23: Well pressure variation depending on gas slippage, diagnostic plot.

We present now the results corresponding to three different flow rates in Fig. 24. We only change the flow rate values: -5,000, -10,000, and -20,000 scf/day. We call attention to the fact that we show the results in the form of the pressure variation (Δp_{wf}) divided by the production flow rate (Q_{sc}), a graph applied in the area of well test analysis. We perceive non-linear behavior through the variation of pressure curves as time progress.

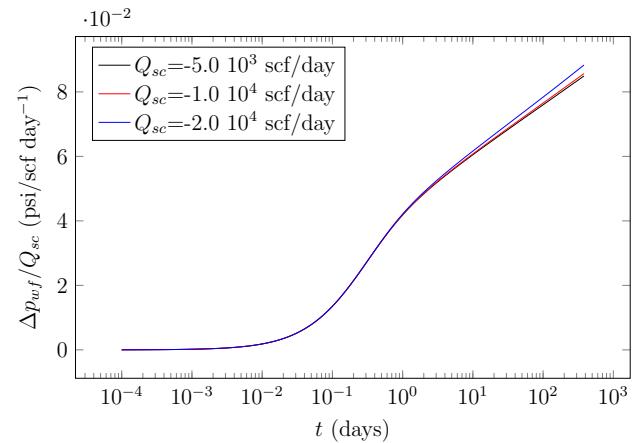


Fig. 24: Variation of the ratio $\Delta p_{wf}/Q_{sc}$ as a function of flow rate.

Figures 25 and 26 display pressure variation curves in a region damaged by contact with fluids external to the reservoir during drilling and completion, and, as a consequence, we have a decreased permeability in this region (it was applied the Hawkins’ formation damage model [39]). We assumed that the damaged region measures 2.77 ft in all tests run.

After the beginning of the transient regime, we can verify a significant variation in pressure drop as the damage increases (the relationship between the permeability of the damaged region, k_s , and the non-damaged region, k). Furthermore, we observe that the effect of storage has a longer duration and magnitude for higher formation damage values (as a result of reduced permeability around the wellbore).

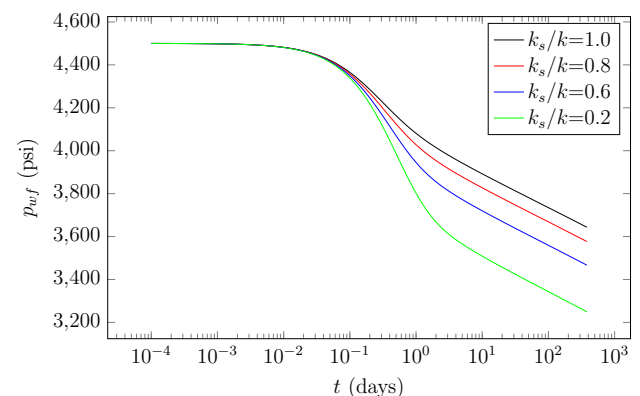


Fig. 25: Well pressure variation due to damage to formation, specialized plot.

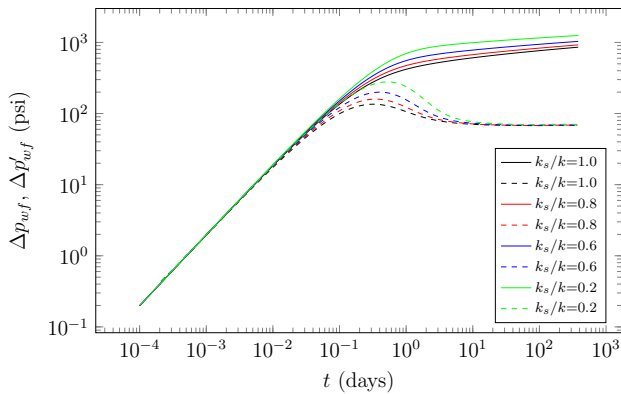


Fig. 26: Wellbore pressure variation due to damage to formation, diagnostic plot.

Finally, to show the appearance of the border effects, even for a shale gas reservoir, we performed a numerical simulation using the data presented in Table 2, except for the following three values: $t_{max}=4,280$ days, $Q_{sc}=-5,000$ scf/day and $L_r=625$ ft.

Therefore, at the end of 12 years of production and after the transient regime, we realize that the pressure curve changes its inclination (downward curvature), Fig. 27, as a result of the emergence of border effects. As we can see, the border effects can (in some cases) appear only after a long period of time. This fact shows the practical difficulty of carrying out well pressure tests, which can take from a few days, in general, to months when long-lasting. Finally, we can also detect the same effect in Fig. 28. It corresponds to the change in the curve slope in the final simulation times, after the horizontal line for the Bourdet derivative.

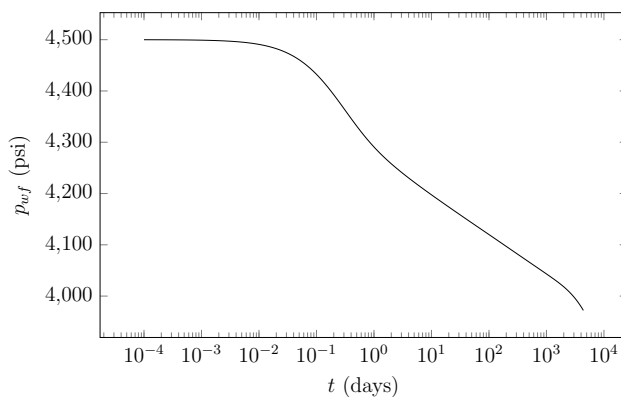


Fig. 27: Well pressure variation due to the appearance of border effects, specialized plot.

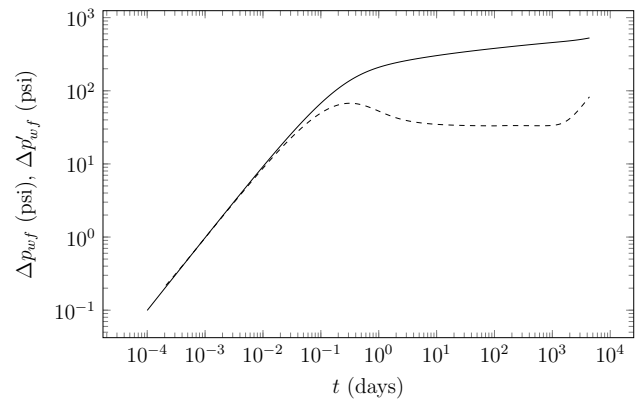


Fig. 28: Wellbore pressure variation due to the appearance of border effects, diagnostic plot.

In all tests performed, the Knudsen number kept its value at $Kn \leq 10$, outside the range of molecular flow.

V. CONCLUSION

We carried out a study to better understand single-phase flow in petroleum reservoirs, aiming to maximize hydrocarbon recovery. The numerical simulation allows testing different production scenarios in less time so that we can choose an optimized production plan that leads to economically viable exploration.

The results of this work showed the importance of applying a complete model (including the effects of slippage, formation damage and wellbore storage) to study single-phase flow in shale gas reservoirs. The use of the classic Darcy's law can lead to well pressure results that do not correspond to reality due to the non-consideration of these effects. This is essential information that must be taken into account if we are to have reservoirs producing and generating profits.

From pressure tests in vertical wells, we could obtain the reservoir properties by solving an inverse problem using the physical model of this work. Therefore, depending on the results, the use of horizontal wells or hydraulic fracturing could make production viable for some reservoirs.

As expected, the nonlinear behavior of the results was adequately detected, especially in cases where we varied the permeability values, which appear explicitly in the governing partial differential equation. Also, we captured the wellbore storage and formation damage effects, expanding the scope of this study, and we verified the influence of these phenomena on

the appearance of the transient flow regime and border effects.

REFERENCES

- [1] Abou-Kassem, J. H., Farouq Ali, S. M., and Islam, M. R. (2006). *Petroleum Reservoir Simulation, A Basic Approach*. Gulf Publishing Company, Houston, USA.
- [2] Al-Attar, H. H. and Barkhad, F. A. (2019). A review of unconventional natural gas resources. *Journal of Nature Science and Sustainable Technology*, 12(4).
- [3] Ali, W. (2012). Modeling gas production from shales and coal-beds. Master's thesis, Stanford University.
- [4] American Public Gas Association (2020). A brief history of natural gas.
- [5] Aziz, M. and Settari, A. (1990). *Petroleum Reservoir Simulation*. Elsevier Applied Science, New York, USA.
- [6] Baruah, H. (1997). *Petroleum and Coal*. M.D. Publications Pvt. Ltd.
- [7] Borgli, F. S., Longa Junior, M. V., and Nunes, I. P. (2008). Remote operations in Bolivia–Brazil gas pipeline - GASBOL. In *International Pipeline Conference*, Atlanta, Georgia, USA.
- [8] Bourdet, D., Ayoub, J. A., and Pirard, Y. M. (1989). Use of pressure derivative in well-test interpretation. *SPE Formation Evaluation*, pages 293–302.
- [9] Bruhn, C. H. L., Gomes, J. A. T., Lucchese Jr., C. D., and Johann, P. R. (2003). Campos basin: Reservoir characterization and management – historical overview and future challenges. In *Offshore Technology Conference*, Houston, Texas, USA.
- [10] Chen, Z., Huan, G., and Ma, Y. (2006). *Computational Methods for Multiphase Flows in Porous Media*. Society of Industrial and Applied Mathematics, Philadelphia, USA.
- [11] Computational Modeling Group (2009). *IMEX, Advanced Oil/Gas Reservoir Simulator*.
- [12] de Souza, G. (2013). *Acoplamento Poço-reservatório na Simulação Numérica de Reservatórios de Gás*. PhD thesis, Universidade Estadual do Norte Fluminense, Macaé, Brasil. In Portuguese.
- [13] Dyrdaahl, J. (2014). Thermal flow in fractured porous media and operator splitting. Master's thesis, Norwegian University of Science and Technology, Trondheim, Norway.
- [14] Empresa de Pesquisa Energética (2006). Plano nacional de energia 2030. In Portuguese.
- [15] Empresa de Pesquisa Energética (2018). Balanço energético nacional. Technical report, Empresa de Pesquisa Energética, Governo Federal, Brasil. In Portuguese.
- [16] Ertekin, T., Abou-Kassem, J. H., and King, G. R. (2001). *Basic Applied Reservoir Simulation*. SPE Textbook Series 7. Society of Petroleum Engineers, Richardson, USA.
- [17] Ezekwe, N. (2011). *Petroleum Reservoir Engineering Practice*. Prentice Hall, Boston, MA, USA.
- [18] Florence, F. A., Rushing, J. A., Newsham, K. E., and Blasingame, T. A. (2007). Improved permeability prediction relations for low permeability sands. In *Society of Petroleum Engineers Rock Mountain Oil & Gas Technology Symposium*, Denver, Colorado, USA.
- [19] Gomes, M. J. (2011). Estudo do mercado brasileiro de gás natural contextualizado ao shale gas. Technical report, Universidade Federal do Rio Grande do Sul. In Portuguese.
- [20] Hamada, G. M. and Singh, S. R. (2018). Mineralogical description and pore size description characterization of shale gas core samples, Malaysia. *American Journal of Engineering Research*, 7(7):1–10.
- [21] Hasan, S., Farooqui, M., Raoand, P., Ramachandran, K., Tripathy, P., and Harinarayana, T. (2013). Petroliferous basins and shale gas – an unconventional hydrocarbon asset of India. *Geosciences*, 3:108–118.

- [22] Jia, B., Tsau, J.-S., and Barati, R. (2018). A workflow to estimate shale gas permeability variations during the production process. *Fuel*, 220:879–889.
- [23] Klinkenberg, L. J. (1941). The permeability of porous media to liquids and gases. *Drilling and Production Practice, American Petroleum Inst.*, pages 200–213.
- [24] Knudsen, B., Whitson, C., and Foss, B. (2014). Shale-gas scheduling for natural-gas supply in electric power production. *Energy*, 78:165–182.
- [25] Lee, A., Gonzalez, M., and Eakin, B. (1966). The viscosity of natural gases. *Journal of Petroleum Technology, Transactions of AIME*, 18(8):997–1000.
- [26] Lee, W. J. and Wattenbarger, R. A. (1996). *Gas Reservoir Engineering*, volume 5. Society of Petroleum Engineers.
- [27] Lenhard, L. G., Andersen, S. M., and Araujo, C. (2018). Energy-environmental implications of shale gas exploration in paran hydrological basin, brazil. *Renewable and Sustainable Energy Reviews*, 90:56–69.
- [28] Li, D., Xu, C., Wang, J., and Lu, D. (2014). Effect of Knudsen diffusion and Langmuir adsorption on pressure transient response in tight- and shale-gas reservoirs. *Journal of Petroleum Science and Engineering*, 124:146–154.
- [29] Li, D., Zhang, L., Wang, J. Y., Lu, D., and Du, J. (2016). Effect of adsorption and permeability correction on transient pressures in organic rich gas reservoirs: Vertical and hydraulically fractured horizontal wells. *Journal of Natural Gas Science and Engineering*, 31:214–225.
- [30] McCain, W. D. (2018). *The Properties of Petroleum Fluids*. PennWell Books, Tulsa, OK, USA, 3rd edition.
- [31] Miao, Y., Li, X., Zhou, Y., Lee, J., Sun, Z., Chang, Y., Wang, S., and Hou, C. (2018). A new rate-transient analysis model for shale gas reservoirs coupled the effect of slip flow and surface diffusion. *International Journal of Heat and Mass Transfer*, 124:1–10.
- [32] Moczydlower, B., Salomo, M. C., Branco, C. C. M., Romeu, R. K., Homem, T. R., Freitas, L. C. S., and Lima, H. A. T. S. (2012). Development of the brazilian pre-salt fields – when to pay information and when to pay for flexibility. In *Proceedings of the Latin American & Caribbean Petroleum Engineering Conference*, Mexico City.
- [33] Nick, H. M., Raoof, A., Gentler, F., Thullner, M., and Regnier, P. (2013). Reactive dispersive contaminant transport in coastal aquifers: Numerical simulation of a reactive Henry problem. *Journal of Contaminant Hydrology*, 145:90–104.
- [34] Palmer, A. (2016). *Introduction to Petroleum Exploration and Engineering*. World Scientific.
- [35] Peaceman, D. (1978). Interpretation of well-block pressures in numerical reservoir simulation. *Society of Petroleum Engineers Journal*, 18(3):183–194.
- [36] Saad, Y. (2003). *Iterative Methods for Sparse Linear Systems*. Society of Industrial and Applied Mathematics, USA.
- [37] Sanjari, E. and Lay, E. N. (2011). An accurate empirical correlation for predicting natural gas compressibility factors. *Journal of Natural Gas Chemistry*, 21:184–188.
- [38] Sutton, R. (1985). Compressibility factors for high-molecular-weight reservoir gases. In *SPE Annual Technical Meeting and Exhibition*, Las Vegas, USA.
- [39] Tavares, C. (2003). Combined effect of non-Darcy flow and formation damage on gas well performance in dual-porosity/dual-permeability reservoirs. Dissertao de mestrado, Colorado School of Mines, Golden, USA.
- [40] Tian, S., Wang, T., Li, G., M., S., Liu, Q., and Zhang, S. (2018). An analytical model for shale gas transport in circular tube pores. *International Journal of Heat and Mass Transfer*, 127:321–328.
- [41] Zheng, S. Y. and Corbett, P. W. M. (2005). Well testing best practice. In *SPE Europe/EAGE Annual Conference*, Madrid, Spain.